Manufacturing Defects in Carbon Fiber-Reinforced Woven Composites made of Repurposed Prepreg Scraps

Luca Sacchetto, Daniela Garcia, Alejandra Castellanos and Paulina Díaz-Montiel

Abstract In recent years, large quantities of carbon fiber-reinforced polymeric (CFRP) composite waste materials have been discarded during the production of composite structures, prompting research investigations into recycling and upcycling. In this article, we present a quantitative investigation of the manufacturing defects present in CFRP composites made of repurposed scraps, and their effect on tensile properties. We manufactured carbon/epoxy woven composite specimens from upcycled prepreg scraps of different sizes using an out-of-autoclave curing method. We captured over a thousand microscopy images of the specimens' microstructure, enabling us to quantify material defects via optical microscopy, scanning electron microscope (SEM), and image processing. Quantified defects include laminate thickness variations, voids, scrap gaps, and resin-rich areas. The effect of different scrap size and scrap layup on the nucleation of these defects was investigated. Experimental testing results show the layup pattern of scraps significantly influences tensile strength, primarily due to the low interfacial normal strength between two adjacent scraps and the high void content. Plates with an overlapping brick-style layup and smaller scrap size exhibited fewer defects and higher tensile strength compared to plates with no overlapping regions and larger scraps.

Luca Sacchetto, Paulina Díaz-Montiel
University of San Diego, 5998 Alcala Park Way, San Diego, CA 92110.
e-mail: lsacchetto@sandiego.edu,pdiazmontiel@sandiego.edu
Corresponding author: Paulina Díaz-Montiel

Daniela Garcia, Alejandra Castellanos
University of Texas El Paso, 500 W University Ave, El Paso, TX 79968

1 Introduction

1.1 Motivation

Released in 2009, the Boeing 787 Dreamliner was the first commercial aircraft with 50% of its structure by weight composed of carbon fiber reinforced polymer (CFRP) composites. This allowed for a 10% reduction in structural weight, resulting in a 6-8% increase in fuel efficiency [1]. The demand for CFRP composites is consistently growing in the aerospace and automotive industries due to their lightweight and excellent mechanical properties, including a high stiffness-to-strength ratio, durability, and high fatigue resistance. The global demand for CFRP reached 199,000 tons in 2022 [2]. This extensive consumption of CFRP composites led to the manufacturing process waste amounting to 36,000 tons in 2020 [3]. By 2050, global waste from CFRP is expected to reach a staggering 500,000 tons [4].

Thermoset epoxy resins are common material choices for the matrix of high-performance CFRP composites. Due to the highly crosslinked nature of polymer chains and networks, epoxy resins cannot be remolded at the end of service life, which poses challenges for the recycling of CFRP composites. While recycling through thermal, chemical, and mechanical decomposition offers potential solutions [5], these technologies are yet to become scalable and cost-effective for CFRP composites. Upcycling efforts, which include repurposing materials (i.e., CFRP scraps) from various stages of a product life cycle, are crucial to address the escalating waste management issue of these materials.

The trade-off of using upcycled CFRP materials is that there is a greater increase of processing defects in the composite's microstructure; hence, these composites exhibit a lower ultimate tensile strength and fatigue life [6]. For this reason, current applications for these upcycled composites have been limited to consumer goods and secondary automotive parts such as side mirrors, door handles, and other internal components [7]. Due to their failure to meet safety regulations, upcycled composites cannot be used in load-bearing engineering applications as they do not meet industry standards. Extending the use of upcycled composites to advanced engineering applications requires a clear understanding of the effect of processing defects on resultant mechanical properties.

1.2 Upcycling of Aerospace Prepreg Scraps

Studies conducted by Barnett et al. [8] and Sultana et al. [1] have investigated the manufacturing and failure of upcycled composites made of randomly-oriented scraps (ROS) made of unidirectional carbon/epoxy prepreg and cured through the Vacuum Bag Only (VBO) process. These studies focused on understanding how scrap and plate geometry (i.e., scrap length, width, plate thickness and aspect ratio) affect stiffness and strength properties. The conclusions presented in the literature have

shown that thinner scrap thickness results in fewer defects and enhances mechanical properties due to the elimination of resin-rich regions [9] [10] and ply waviness [11], which are manufacturing defects caused by overlapping scrap ends. It has also been observed that an increase in scrap length minimizes defects at scrap gaps and overlaps regions and results in longer continuous fibers that increase the strength in the longitudinal direction [1].

1.3 Defects and Failure Mechanisms in Randomly-Oriented Scrap Composites

Selezneva and Lessard studied the quantification of scrap overlaps and gap regions in ROS composites, aiding in the comprehension of the progressive failure of these materials [9] under different loading condition . This investigation studied carbon/epoxy plates made of discontinuous, randomly-oriented scraps of unidirectional tape manufactured in compression molding. The plates consisted of scraps of different sizes and laminate thicknesses. Tensile, compression, in-plane shear, and fatigue tests were carried out. Post-experimentation, the findings revealed a significant difference in the mechanical properties of the composite plates with long (50 mm) scraps compared to shorter (6 mm) scraps. The optical imaging showed a substantial increase in resin-rich regions in the ROS composites of short scrap signifying epoxy resin buildup in scrap gap regions where two scrap met. There was also significant distortion in the scraps for the ROS composites of short scrap, however, neither of these two defects were quantified. Tensile testing showed a 60% decrease in strength for the short-scrap plates compared to the longer scraps. Post-mortem optical microscopy imaging revealed two dominant failure modes: strand fracture and debonding. Scrap fracture occurred at greater strains in the long ROS scrap composites, showing the durability these plates under tensile testing. Optical imaging of tested coupons shows that cracks propagate in the shortest scrap overlapping region. Longer scrap overlap over a greater distance, allowing cracks to propagate further prior to failure.

The studies above have enhanced our understanding of composites made from discontinuous scraps, laying the groundwork for optimizing upcycled composite manufacturing processes. These studies have shown a significant reduction in mechanical properties and increased variability, which is influenced by scrap geometry, particularly longitudinal length and thickness. These factors affect the nucleation of defects such as resin-rich regions and voids, composite's microstructure, and the resultant mechanical performance. The present paper focuses on further understanding the impact of manufactured defects on the composite mechanical performance by providing a detailed characterization and quantification of defects, and showing how defects vary given the layup and scrap size.

1.4 Objectives, Structure and Scope

The objectives of this article are: 1) investigate how scrap size and scrap layup influence the nucleation of processing-induced defects in upcycled CFRP composites; 2) characterize and quantify these defects; and 3) evaluate the effect of these defects on the tensile properties. The detailed characterization and quantification of process-induced defects, which is currently lacking in published literature, will be essential for advancing the understanding of the microstructure-property-performance relationship of upcycled CFRP composites. Additionally, studies on how variations in scrap size and layup can result in various processing defects will inform the manufacturing, design, and analysis of future upcycled CFRP composite structures.

2 Methods

2.1 Manufacturing and Specimen Preparation

Two 12 x 6 inch (304.8 x 152.4 mm) composite plates (6-ply thick) were manufactured out of discontinuous scraps. All plates were made up of the same carbon/epoxy woven prepreg (Cycom 5320-1 T650-35 3K 8HS Fabric 36% RW), which was expired and donated to the university. To control the nucleation of processing-defects and study the effect of scrap size and layup on mechanical properties, the discontinuous scraps were oriented in the same direction with the warp aligned with the loading direction.

The only variables that changed between the two composites were the scrap size and scrap layup. The first plate was made up of 1 x 0.5 inch (25.4 x 12.7 mm) rectangular scraps using approximately 144 scraps per ply. The scraps were laid out in an overlapping, brick-style manner, which repeated every other ply (z-direction) as shown in Figure 1 (a). In the figure, the length of the scrap is L while the width is w. The second plate was made up of 1 x 1 inch (25.4 x 25.4 mm) square scraps, and each ply was composed of about 66 scraps. The scraps in the second plate were shifted only in the y-direction as shown in Figure 1 (b).

After the layup, the plates were vacuum-sealed and cured in an oven following the specific curing guidelines provided by the manufacturer [12]. Keeping the curing process, number of plies, and size of the plates consistent was important in increasing accuracy and validity of the experiments.

Fiberglass tabs were glued onto the composite plates using structural adhesive. Once the tabbing process was complete, 1-inch wide by 12-inch long (25.4 x 304.8 mm) coupons were cut and five coupons were produced by each plate. All of the following manufacturing, specimen preparation, and testing procedures were defined and followed by the ASTM D3039-17 Standard [13].

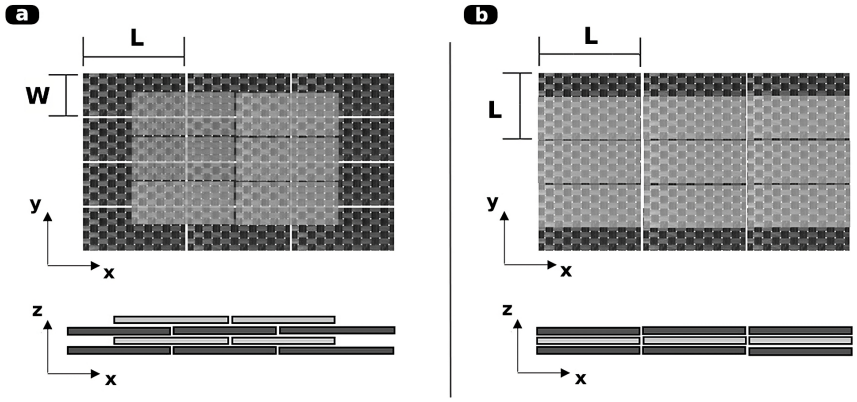

Fig. 1 Plate layups considered in this study: (a) Plate 1 shifts by half the width W and length L of a scrap in the respective y- and x-directions, every other ply. (b) Plate 2 shifts only in the y-direction by $L/2$, and there is no shift in the x-direction.

2.2 Characterization and Quantification of Defects

To understand how the scrap layup and scrap size affect the mechanical properties, quantifying the defects present at the microstructure is essential. Defects that were characterized and quantified include scrap gap regions, voids, and resin-rich regions. These defects were analyzed by examining the cross-section of all the manufactured composite coupons via optical microscopy. Collages were created from the gathered pictures to image the cross-section of each coupon. Considering both front and back faces, two collages per coupon were created. However, for quantifying defects, only a four-inch section of the cross-section of each coupon was used in the analysis. Image processing was performed using the commercial software Photoshop™.

With respect to the total cross-sectional area, the relative content of resin-rich regions (a_{rrr}), voids (a_v), and scraps (a_s) were determined using Eqs. 1-3.

$$(1) \quad a_s = \frac{A_s}{A_{\text{total}}} \qquad \text{(Scrap area fraction)}$$

$$(2) \quad a_{rrr} = \frac{A_{rrr}}{A_{\text{total}}} \qquad \text{(Resin-rich regions area fraction)}$$

$$(3) \quad a_v = \frac{A_v}{A_{\text{total}}} \qquad \text{(Void area fraction)}$$

The calculations for Eqs. 1-3 assumed that the cross-sectional surface area of the composite coupons, using a consistent length of 2 inches, corresponds to A_{total}. The area of resin-rich regions (A_{rrr}) was quantified automatically through the Photoshop color range selection tool to identify and measure the area occupied by all resin-rich

regions within A_{total}. The area of voids (A_v), excluding microvoids, were manually selected using Photoshop's brush tool to highlight voids, and their respective pixel coverage was calculated using the histogram tool. Due to their small pixel coverage, microvoids were disregarded in the quantification process to accommodate for human error when quantifying the volume fraction of voids. This shortcoming is addressed in the Conclusions and Future Work (Section 4). Finally, the area of scraps (A_s) was calculated by subtracting A_{rrr} and A_v from A_{total}.

2.3 Experimental Setup

The electromechanical Instron 3382 universal testing system (UTS), shown in Figure 2, was utilized to conduct tensile testing. Since one coupon per plate was destroyed for SEM imaging, only four coupons from each plate were tested. Coupon 2B failed during the setup of the tensile experiment, and its data is therefore excluded from the analysis. To further validate the test results considering ASTM standards [13], we have extended our manufacturing efforts and are currently testing ten additional coupons. Further details are provided in Conclusions and Future Work (Section 4).

To minimize variations due to environmental factors, all coupons were tested on the same day and under identical conditions. A two-inch gauge length extensometer was used to measure the local deformations in the composite coupons. The displacement rate was set to 2 mm/min and no pre-load was added prior to testing. The UTS machine was programmed to stop once ultimate tensile failure occurred.

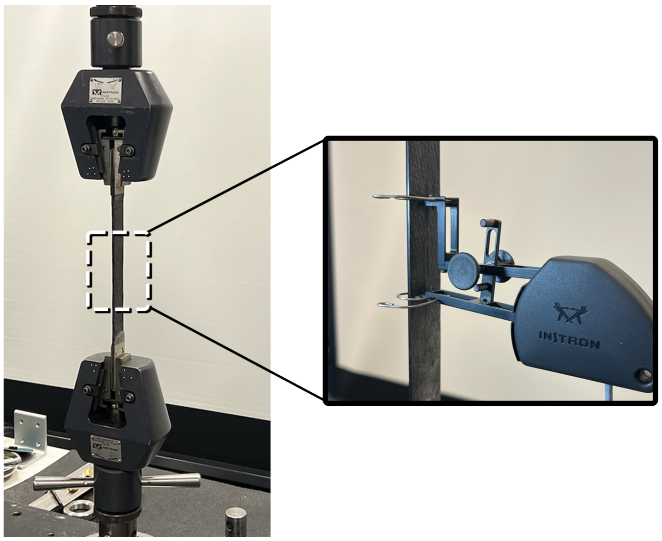

Fig. 2 Image of the experimental setup. An extensometer was utilized for measuring the local deformations during testing.

3 Results and Discussions

A representative image of the cross-section of a composite coupon (Plate 2 type) can be observed in Figure 3. From this image, the main defects found can be identified as: (a) dark patches of resin buildup; (b) circular voids represented by white circles; (c) interlamina voids, which are located between the faces of two scraps; (d) complete voids, or visible holes present within the microstructure; and (e) micro-voids, which resemble circular voids but have diameters of 20 μm or less. Circular voids shown in the microstructure were confirmed to be voids after further inspection under scanning electron microscope (SEM) imaging, as shown in Figure 4.

Fig. 3 Characterization of defects observed in the cross-sectional area of the composite coupons: (a) resin-rich region, (b) circular void, (c) interlaminar void, (d) complete void, and (e) micro void. The optical imaging corresponds to composite coupon 2B1 (Plate 2).

Results from the defect fraction analysis, summarized in Tables 1 and 2, indicate that the resin-rich regions (RRR) for Plate 1 averaged 11.0% with a standard deviation of 2.4%, while Plate 2 exhibited a similar average of 11.3%. However, Plate 2's standard deviation was double that of Plate 1, at 4.10%. The primary discrepancy between the two plates was observed in the area fraction of voids. Plate 1 averaged only 0.71%, whereas Plate 2 showed a 6x increase from Plate 1 at 4.44%. Consequently, the area fraction of Plate 1's scraps, was calculated to be 88.3%, whereas Plate 2's was 84.3%, reflecting approximately 4% difference.

The resin-rich region content, formed by the accumulation of epoxy resin during the curing process, explain the similar laminate thickness values observed in the two plate types. Plate 1 and Plate 2 show laminate thickness values of 8.06×10^{-2} inches (2.05 mm) and 7.87×10^{-2} inches (2.00 mm), respectively. The similar laminate thickness between the two plates indicates a consistent thickness of the individual plies, resulting in comparable resin-rich region content in both plates. This correlation between ply and laminate thickness and the content of resin-rich regions has also been reported in the past [11].

The void content in Plate 1 differs significantly with Plate 2. The largest voids observed in Plate 1 are inter-laminar voids approximately 100 μm in diameter, while

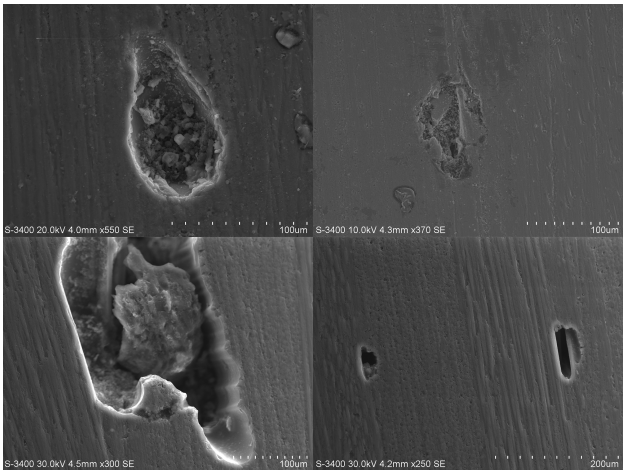

Fig. 4 Scanning Electron Microscope (SEM) images showing circular and microvoids within the cross-section of the composite coupons. The figures correspond to images captured of specimens 1E (Plate 1) and 2E (Plate 2).

Table 1 Quantification of defects in Plate 1, specimens A-E

Plate 1	RRR (%)	Voids (%)	Sraps (%)
Average	11.0	0.71	88.3
Maximum	13.9	1.37	90.8
Minimum	8.23	1.95×10^{-2}	85.0
Standard Deviation	2.40	0.60	2.60

Table 2 Quantification of defects in Plate 2, specimens A-E

Plate 2	RRR (%)	Voids (%)	Sraps (%)
Average	11.3	4.44	84.3
Maximum	17.1	5.44	90.3
Minimum	6.35	3.39	78.3
Standard Deviation	4.10	0.700	4.60

the most common voids in Plate 2 are circular voids with an average diameter of 400 μm, as shown in Figure 5. Although the shape of voids is consistent across both plates, the surface area covered by circular voids in Plate 2 contributes to a 4% increase in the area fraction of voids.

The hypothesis that scrap layup influences the area fraction of voids is supported through optical imaging, which reveals that most defects appear between the two ends of scraps. An average gap distance of 7.09×10^{-3} inches (0.180 mm) and 9.36×10^{-3} inches (0.238 mm) exist between the scraps of Plates 1 and 2, respectively. The gap distances between scraps in these two plates are quantified in Table 3 and Table 4. The voids present in these scrap gap regions (Figure 5) are more pronounced and

larger in the parallel scrap layup of Plate 2 compared to the overlapping brick-style layup in Plate 1. The large voids present between scraps in Plate 2 are concluded to be a result of non-uniform resin flow during the curing process. The absence of overlapping scraps allows resin to flow downward without obstruction, causing the formation of voids as the resin solidifies. This is not the case for the curing in Plate 1 as the bottom overlapping brick-style layup of scraps results in a more uniform resin flow in the horizontal direction eliminating the possibility for resin to flow downwards due to gravitational pulls. As a result, Plate 1 exhibits a higher prevalence of interlaminar voids compared to circular voids between scraps, whereas Plate 2 shows the opposite trend.

Table 3 Quantification of scrap gap distances in plate 1, specimens A-E

Plate 1	Scrap Gap Distance (inches)	Scrap Gap Distance (mm)
Average	7.09×10^{-3}	1.80×10^{-1}
Maximum	1.54×10^{-2}	3.92×10^{-1}
Minimum	1.47×10^{-3}	3.74×10^{-2}
Standard deviation	3.38×10^{-3}	8.60×10^{-2}

Table 4 Quantification of scrap gap distances in Plate 2, specimens A-E

Plate 2	Scrap Gap Distance (inches)	Scrap Gap Distance (mm)
Average	9.36×10^{-3}	2.38×10^{-1}
Maximum	2.05×10^{-2}	5.21×10^{-1}
Minimum	2.42×10^{-3}	6.15×10^{-2}
Standard deviation	4.26×10^{-3}	1.08×10^{-1}

Tables 5 and 6 summarize the experimental testing results of Plate 1 and 2, respectively. The table shows results of stiffness, strength and displacement at failure values for these two plates. The stress-strain curves of Plates 1 and 2 are provided in Figure 6 and 7, respectively.

The experimental results reveal that Plate 1 exhibited the highest mechanical properties, with an average ultimate tensile strength of 43.8 ksi (302 MPa), an average peak load of 3.87 kips (17.2 kN), and average displacement at failure of 0.51 inches (13.0 mm). Conversely, Plate 2 displayed significantly lower mechanical properties, with an average tensile strength of 8.27 ksi (57.0 MPa), an average peak load of 7.93×10^{-1} kips (3.52 kN), and an average failure displacement of 1.07×10^{-1} inches (2.72 mm), represented in Figure 7.

Despite the significant differences in strength values between Plate 1 and Plate 2, the average stiffness values are comparable. The average stiffness of Plate 1 specimens is 8.8 Msi, while Plate 2 specimens is 7.95 Msi. Compared to tension strength quasi-isotropic continuous-fiber laminates made of the same carbon/epoxy

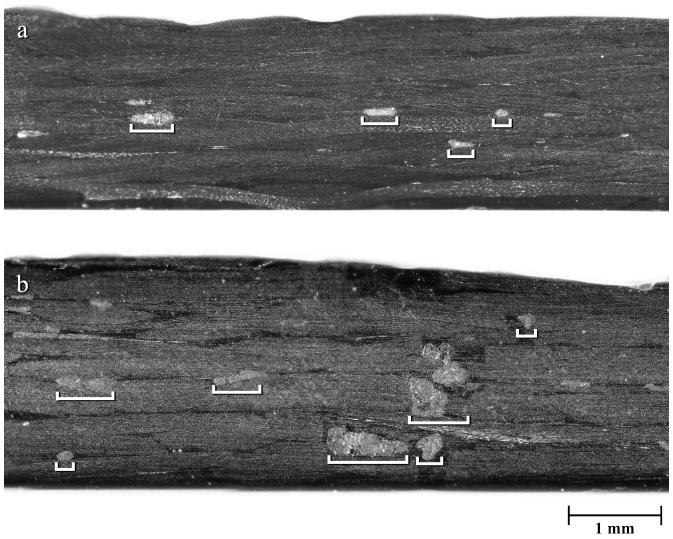

Fig. 5 Optical imaging of (a) Plate 1 specimen 1B2 and (b) Plate 2 specimen 2B2, comparing void dimensions. Plate 1 exhibits a higher content of interlaminar voids, while Plate 2 predominantly has larger circular voids.

system (96 ksi as provided by the manufacturer [12]), the strength of all specimens is significantly reduced. However, the stiffness values of both Plate 1 and 2 are consistent to the values reported by the manufacturer (9 Msi). This implies that for applications where composites must be designed based on stiffness, composite laminates made of repurposed discontinuous prepreg scraps could be an alternative material choice.

Notable cracking noises occurred during testing of Plate 1 specimens, which can be explained with transverse matrix cracking damage. On the other hand, Plate 2 specimens showed minimal matrix cracking during testing as they did not emit notable sounds prior to the ultimate failure of the coupons. This indicates that the failure mechanisms in these two composite plates are fundamentally different and need to be investigated further. Figure 8 highlights the tensile test failure modes observed at each specimen of Plate 1.

The experimental results of Plate 1 show that specimens 1A and 1C exhibited similar tensile strength and displacement at failure values. Specimens 1B and 1D also showed similar tensile strength and displacement at failure values. However, compared to specimens 1A and 1C, the average strength values of specimens 1B and 1D were approximately 25% lower. The average displacement at failure values of specimens 1B and 1D were also lower by approximately 39%.

To explain these two distinct failure responses between specimens 1A and 1C and specimens 1B and 1D, postmortem imaging of the cross-section of the coupons after testing was conducted (Figure 9). Analysis of these images indicates that the samples

Table 5 Summary of experimental testing results of Plate 1 specimens

Specimen	Peak load (kip)	Stiffness (Msi)	Strength (ksi)
1A	4.40	8.07	50.3
1B	3.47	10.6	39.1
1C	4.32	7.58	49.6
1D	3.30	8.92	36.0
Average	3.87	8.80	43.8
Maximum	4.40	10.6	50.3
Minimum	3.30	7.58	36.0
St. dev.	1.74	1.33	7.28

Table 6 Summary of experimental testing results of Plate 1 specimens

Specimen	Peak load (kip)	Stiffness (Msi)	Strength (ksi)
2A	0.793	7.05	9.0
2B	-	-	-
2C	0.593	8.63	6.8
2D	0.897	8.18	10.0
Average	0.761	7.95	8.6
Maximum	0.897	8.63	10.0
Minimum	0.593	7.05	6.8
St. dev.	0.155	0.81	1.64

exhibited two possible failure patterns, as shown in the schematic at the bottom of Figure 9. Case 1 failure is associated to a crack propagating through the resin-rich regions in between adjacent scraps, while Case 2 failure represents scrap and fiber fracture. It is possible that Case 1 fracture initiates at surface defects of outer plies, and traverses through the thickness of the composite. Case 2 fracture can initiate at internal defect that act as high stress concentration sites and trigger crack nucleation and growth.

It can be observed from the post-mortem microscopy images in Figure 9 that specimens 1B and 1D predominantly exhibited Case 1 failure, showing multiple failure mechanisms that include delamination cracks, tow pull-out, matrix cracking, and scrap/fiber fracture. On the other hand, specimens 1A and 1C experienced Case 2 failure, showing failure mechanisms such as fiber fracture, transverse matrix cracking, and small delamination cracks between adjacent scraps. Consideration must be taken into account that these two failure cases are simplified explanations of the crack propagation experienced as specimens likely encountered a combination of both cases. For instance, Figure 9 (a) shows specimen 1A with debonding at the top and bottom of the lamina, but brittle fiber fracturing in the center plies. Additionally, the 3D nature of the crack propagation phenomena requires further analysis of the

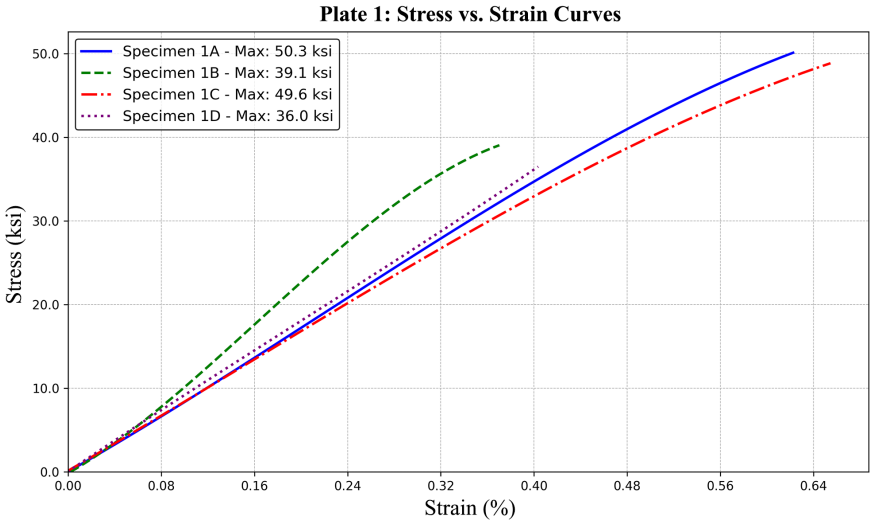

Fig. 6 Stress vs. Strain curves for Plate 1 specimens. Each curve is smoothed using polynomial interpolation, and the legend indicates the maximum stress value for each specimen.

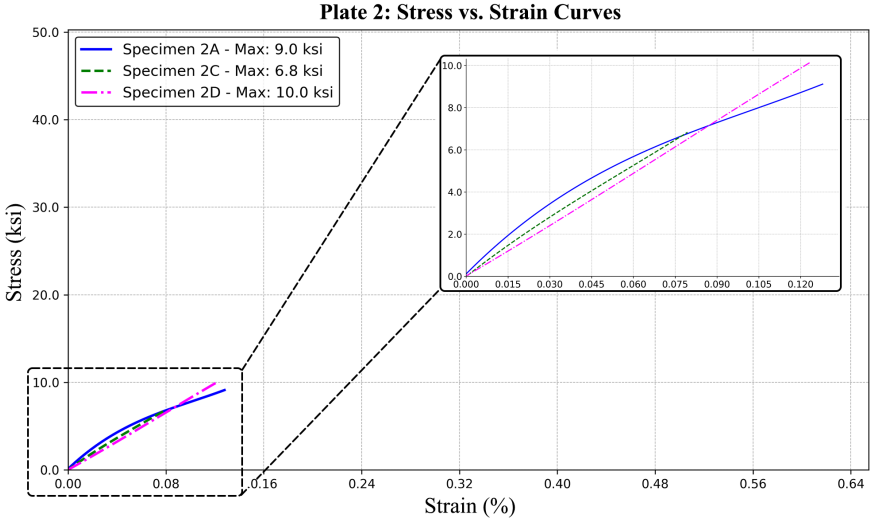

Fig. 7 Stress vs. Strain curves for specimens from Plate 2. Each curve is smoothed using polynomial interpolation, and the legend indicates the maximum stress value for each specimen.

fracture surface through the width of the laminates to fully understand the interaction with other failure mechanism.

The failure morphology for all Plate 2 specimens leads to the conclusion that the failure location initiated at one of the large circular voids present in between the

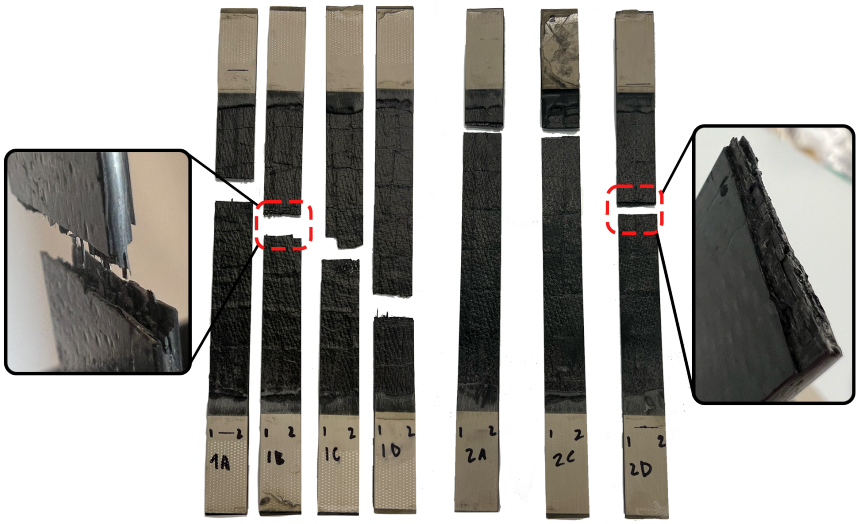

Fig. 8 Failed coupons from tensile testing, showing specific failure locations for each specimen.

ends of two adjacent scraps. The parallel alignment of scraps (along the z-direction) between each lamina did not allow the crack to propagate throughout the scraps and fracture the fibers. Instead, the load remained locally concentrated at the resin-rich region between scraps. Despite Plate 2 only having a 4.01% greater porosity compared to Plate 1, the tensile strength was significantly reduced by 81.03%. Our findings concluded that the significant difference in tensile strength between the two plates can be attributed to the different crack propagation phenomena experienced by Plate 2 specimens.

Figure 10 (a) and (b) show a comparison of the postmortem microscopy images of Plate 1 and Plate 2, respectively. The top images illustrate the microscopy images before failure. The bottom images present cross-sections of the specimens after tensile failure. Marking 1 compares the increased size of complete voids present at the failure location of 1B. Marking 2 shows the opposite end of the specimen where a scrap detached from the composite due to cracking at a resin-rich region on the right side of a scrap. Marking 3 indicates a cluster of microvoids concentrated that resulted in crack nucleation at this site. Marking 4 shows the opposite end of this scrap where the specimen split due to crack at a large complete void.

Postmortem imaging on the tested specimens confirms the location of possible crack initiation site for Plate 2 at regions of void clusters within the scrap gap regions. Meanwhile, Figure 10 (a) shows that Plate 1 cracks nucleated due to a combination of complete voids and resin-rich regions. In the bottom image of Figure 10 (a) tow pull-out and extensive delamination between plies can be clearly identified in the split coupon. The delamination crack propagation distance is 1.925×10^{-1} inches (4.89 mm). At the far left of this failure point, there are complete voids, each a few micrometers long. The image below shows these same voids noticeably enlarged,

suggesting a possible location where crack initiation may have occurred. The crack then propagated through the surrounding resin-rich regions, ultimately causing the failure of the coupon. Meanwhile, in the top image of Figure 10(b) the presence of complete, circular, and smaller interlamina voids can be observed, which caused the crack propagation. In contrast to Plate 1, the crack propagation distance of Plate 2 was only 7.48×10^{-2} inches (1.90 mm), which is a 61.16% decrease in delamination crack extent when compared to that of Plate 1.

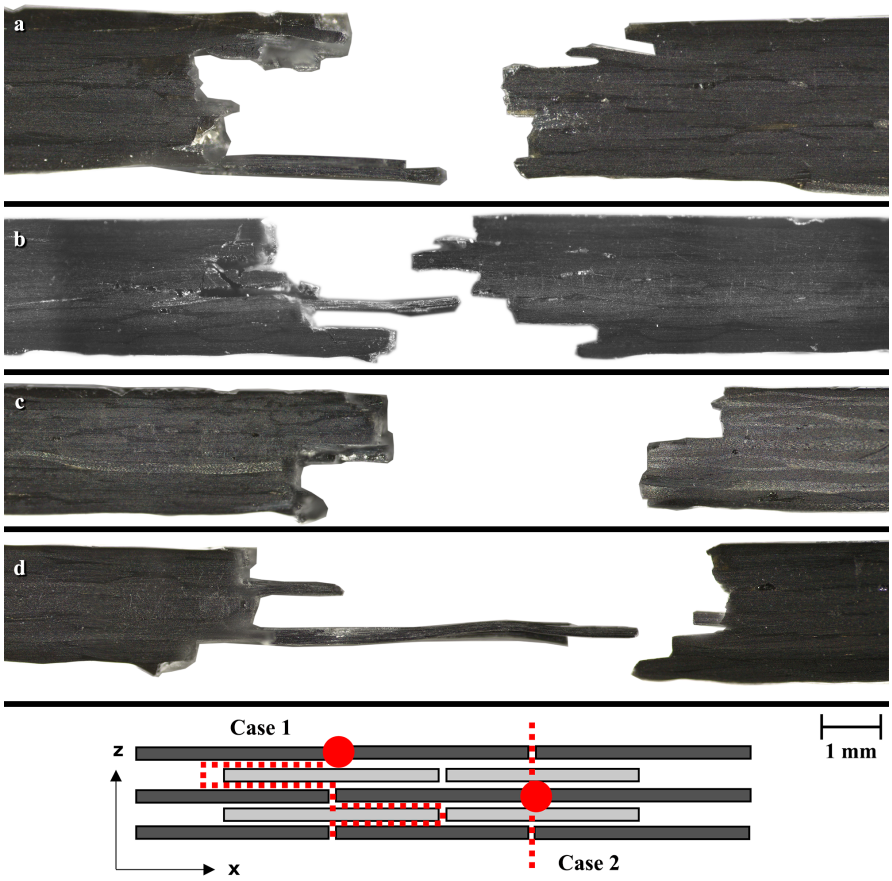

Fig. 9 Postmortem imaging of Plate 1, specimens 1A to 1D. The schematic at the bottom illustrates the two failure mechanisms observed in Plate 1 specimens: scrap debonding (case 1) and scrap fracturing (case 2). The dotted red lines through the cross-section show the possible crack propagation pattern. Specimens (a)1A and (c)1C exhibited a combination of Case 1 failure but primarily Case 2 failure. In contrast, specimens (b)1B and (d)1D displayed only Case 1 failure.

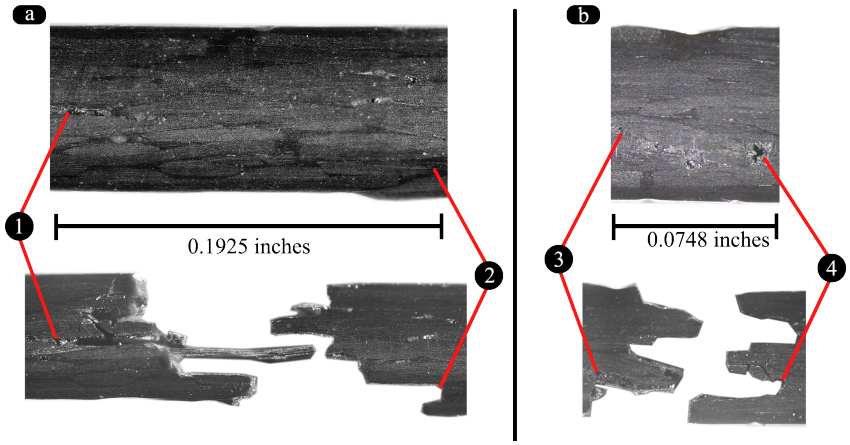

Fig. 10 Postmortem imaging of (a) specimen 1B and (b) specimen 2D.

4 Conclusions and Future Work

Plate 1 exhibits the most optimal layup (overlapping brick-style) among the two plates that considers a scrap shift in both the x and y directions every other ply. This arrangement of scraps yields the lowest content of defects at 11.73%. This layout also facilitates even distribution of tensile load throughout the composite due to its continuously overlapping scraps, leading to an average ultimate tensile strength of 43.8 ksi (302 MPa). Conversely, Plate 2 demonstrates a poor layout style, that being a shift in the y direction only, as cracks struggle to propagate through the parallel alignment of scraps in the x direction. This results in a very weak average tensile strength of 8.27 ksi (57.0 MPa). The quantification of volume fractions shows a 3.73% increase in the volume fraction of voids in Plate 2, compared to the volume fraction of plate 1 being only 0.71%. The most prominent voids in Plate 2 included circular and complete voids which were present in the gap regions between adjacent scraps. This region between adjacent scraps also acts as the failure initiation site for Plate 2 the coupons. Meanwhile, Plate 1 showed higher interlaminar voids content.

The experimentation conducted in this project shows the critical effect scrap layup has on the tensile properties of a composite material, particularly those made from repurposed prepreg scraps. Consciously devising optimized methods for stacking scraps not only enhances mechanical properties but can extends the lifespan of these repurposed materials. Understanding how the layup pattern influences defect formation and resultant mechanical properties, allows us to mitigate the knockdown in load-carrying capacity. The conclusions present in our paper relate to the empirical results with earlier works on ROS presented in the literature, advancing the understanding of the effect of processing defects on the mechanical properties of upcycled composites.

Our research group is committed to continuing the research studies introduced in this paper. We hope to answer the shortcomings of our experimentation with the manufacturing of more plates with various scrap sizes and test other scrap layups. By manufacturing additional composite plates, we will be able to conduct more tensile tests on Plates 1 and 2 type specimesn, thereby obtaining more accurate results on the detailed quantification of defects and mechanical properties under tensile loading. Finally, our team also plans on utilizing the data gathered throughout this research study to conduct a finite element analysis of the same upcycled composites. These computational efforts will contribute to the understanding of stress distribution and damage initiation in these upcycled carbon fiber scrap composites. Our objective is to inform the experimental findings presented in the current investigation.

5 Acknowledgements

Author L. Sacchetto and P. Díaz-Montiel thank Mr. Russel Harrel and Dr. Lisa Baird (University of San Diego) for their assistance with optical microscopy and SEM imaging. We thank Dr. Satchi Venkataraman and Dr. Adrian Rivera (San Diego State University) for facilitating the tension testing of the coupons. Finally, we are deeply appreciative of the students in Dr. Diaz-Montiel's class (MENG-494: Composite Materials) for their contributions to the manufacturing of the upcycled composite plates used throughout the study. This research was partially supported by the Kern Entrepreneurial Engineering Network (KEEN).

References

1. S. Sultana, A. Asadi, J. Colton, K. Kalaitzidou, Composites made from cf prepreg trim waste tapes using sheet molding compounds (smc) technology: Challenges and potential, Composites Part A: Applied Science and Manufacturing 134 (2020) 105906. doi:https://doi.org/10.1016/j.compositesa.2020.105906.
   URL https://www.sciencedirect.com/science/article/pii/S1359835X20301445
2. M. Sauer, M. Kuhnel, Composites market report 2019, Carbon Composites 2 (2019) 1–11.
3. P.-Y. Chen, R. Feng, Y. Xu, J.-H. Zhu, Recycling and reutilization of waste carbon fiber reinforced plastics: Current status and prospects, Polymers 15 (17) (2023). doi:10.3390/polym15173508.
   URL https://www.mdpi.com/2073-4360/15/17/3508
4. A. Lefeuvre, S. Garnier, L. Jacquemin, B. Pillain, G. Sonnemann, Anticipating in-use stocks of carbon fiber reinforced polymers and related waste flows generated by the commercial aeronautical sector until 2050, Resources, Conservation and Recycling 125 (2017) 264–272.
5. J. Zhang, V. S. Chevali, H. Wang, C.-H. Wang, Current status of carbon fibre and carbon fibre composites recycling, Composites Part B: Engineering 193 (2020) 108053.
6. G. Nilakantan, S. Nutt, Reuse and upcycling of thermoset prepreg scrap: Case study with out-of-autoclave carbon fiber/epoxy prepreg, Journal of Composite Materials 52 (3) (2018) 341–360. arXiv:https://doi.org/10.1177/0021998317707253, doi:10.1177/0021998317707253.
   URL https://doi.org/10.1177/0021998317707253

7. G. Nilakantan, S. Nutt, Reuse and upcycling of aerospace prepreg scrap and waste, Reinforced Plastics 59 (2015) 44–51. doi:10.1016/j.repl.2014.12.070.
8. P. Barnett, C. Gilbert, D. Penumadu, Repurposed/recycled discontinuous carbon fiber organosheet development and composite properties, Composites Part C: Open Access 4 (2021) 100092. doi:10.1016/j.jcomc.2020.100092.
9. M. Selezneva, L. Lessard, Characterization of mechanical properties of randomly oriented strand thermoplastic composites, Journal of Composite Materials 50 (20) (2016) 2833–2851. arXiv:https://doi.org/10.1177/0021998315613129, doi:10.1177/0021998315613129.
URL https://doi.org/10.1177/0021998315613129
10. M. Selezneva, S. Roy, L. Lessard, A. Yousefpour, Analytical model for prediction of strength and fracture paths characteristic to randomly oriented strand (ros) composites, Composites Part B: Engineering 96 (2016) 103–111. doi:https://doi.org/10.1016/j.compositesb.2016.04.017.
URL https://www.sciencedirect.com/science/article/pii/S1359836816302414
11. Y. Li, S. Pimenta, J. Singgih, S. Nothdurfter, K. Schuffenhauer, Experimental investigation of randomly-oriented tow-based discontinuous composites and their equivalent laminates, Composites Part A: Applied Science and Manufacturing 102 (2017) 64–75. doi:https://doi.org/10.1016/j.compositesa.2017.06.031.
URL https://www.sciencedirect.com/science/article/pii/S1359835X17302567
12. Solvay, CYCOM® 5320-1 PREPREG, Solvay (2016).
13. A. International, D3039/D3039M-17: Standard test method for tensile properties of polymer matrix composite materials. (2019).